RMetS
Royal Meteorological Society

Synchronisation of the equatorial QBO by the annual cycle in tropical upwelling in a warming climate

Kylash Rajendran,[a]* Irene M. Moroz,[a] Peter L. Read[b] and Scott M. Osprey[b]
[a]*Mathematical Institute, University of Oxford, UK*
[b]*Atmospheric, Oceanic and Planetary Physics, University of Oxford, UK*

*Correspondence to: K. Rajendran, Mathematical Institute, University of Oxford, Andrew Wiles Building, Radcliffe Observatory Quarter, Oxford OX2 6GG, UK. E-mail: rajendran@maths.ox.ac.uk

The response of the period of the quasi-biennial oscillation (QBO) to increases in tropical upwelling are considered using a one-dimensional model. We find that the imposition of the annual cycle in tropical upwelling creates substantial variability in the period of the QBO. The annual cycle creates synchronisation regions in the wave forcing space, within which the QBO period locks onto an integer multiple of the annual forcing period. Outside of these regions, the QBO period undergoes discrete jumps as it attempts to find a stable relationship with the oscillator forcing. The resulting set of QBO periods can be either discrete or broad-banded, depending on the intrinsic period of the QBO.

We use the same model to study the evolution of the QBO period as the strength of tropical upwelling increases, as would be expected in a warmer climate. The QBO period lengthens and migrates closer towards 36- and 48-month locking regions as upwelling increases. The QBO period does not vary continuously with increased upwelling, however, but instead transitions through a series of two- and three-cycles before becoming locked to the annual cycle. Finally, some observational evidence for the cyclical behaviour of the QBO periods in the real atmosphere is presented.

Key Words: QBO; synchronisation; Brewer–Dobson circulation; climate change

Received 1 July 2015; Revised 12 November 2015; Accepted 18 November 2015; Published online in Wiley Online Library 9 February 2016

1. Introduction

The quasi-biennial oscillation (QBO) is the dominant mode of variability in the equatorial stratosphere (Baldwin *et al.*, 2001). It consists of alternating intervals of westerly and easterly zonal mean winds that originate around 5 hPa and descend to the tropopause at 100 hPa. The period of the system ranges between 22 and 34 months, with an average of 28.5 months (Pascoe *et al.*, 2005). The oscillation arises as the result of a wave–mean flow interaction between the background stratospheric winds and a wide variety of tropospheric equatorial waves (Lindzen and Holton, 1968; Holton and Lindzen, 1972). As these waves propagate vertically through the stratosphere, they dissipate and deposit momentum into the mean flow. Wave dissipation tends to maximise near critical layers, defined as heights in the stratosphere where a wave's Doppler-shifted frequency $k(\bar{u} - c)$ approaches zero. Hence, certain combinations of waves can create different zonal accelerations in height that change as the mean flow evolves, allowing for the creation of an oscillation in the zonal wind (Plumb, 1977).

It has long been held that the QBO is somewhat coupled to the annual cycle (Dunkerton and Delisi, 1985; Dunkerton, 1990). The onset of westerly QBO regimes at 44 hPa occurs preferentially during Northern Hemisphere summers, while easterly wind onsets at 20 hPa tend to occur around Northern Hemisphere winters (Pascoe *et al.*, 2005). The QBO periods have also been shown to adopt a bimodal distribution of either 24 or 30 months at 5 hPa (Kuai *et al.*, 2009), which may be due in part to synchronisation of the QBO and the stratopause semi-annual oscillation (Dunkerton and Delisi, 1997; Read and Castrejón-Pita, 2012).

It has been proposed that the annual cycle in the Brewer–Dobson circulation could be responsible for the observed seasonal synchronisation of the QBO (Kinnersley and Pawson, 1996; Hampson and Haynes, 2004). The Brewer–Dobson circulation induces a vertical upwelling of stratospheric air at the Equator. This results in the vertical advection of zonal winds, which impedes the descent of QBO wind regimes and increases its period (Saravanan, 1990; Dunkerton, 1991). As the strength of the upwelling varies with the annual cycle (Yulaeva *et al.*, 1994), this allows for the QBO's descent rate (and hence its period) to be modulated by the annual cycle.

Numerous climate model projections have predicted that the strength of tropical upwelling will increase at a rate of between 2 and 3.2% per decade as a result of increased greenhouse gas

emissions (Butchart, 2014, and references therein). The effect that this increase might have on the period of the QBO is unclear (Schirber *et al.*, 2015). Although one would naturally expect increased upwelling of tropical air to delay the descent of QBO winds, increased convective wave activity in the Tropics due to changes in sea surface temperatures in a warming climate might simultaneously enhance tropical wave activity, which generally tends to increase the descent rate and decrease the period of the QBO (Li *et al.*, 1997). Nevertheless, if one assumes that the increase in upwelling is the dominant forcing in a future climate, it would be instructive to study how the QBO period would change as a result of this increase.

In this article we use a one-dimensional idealised model of the QBO to investigate its synchronisation by the annual cycle in tropical upwelling, as well as the QBO response to increased tropical upwelling in a warming climate (Butchart *et al.*, 2006; Garcia and Randel, 2008). Since comprehensive climate models still encounter difficulties in generating realistic QBOs (e.g. Yao and Jablonowski, 2015), there is some utility to be gained from studying this question in the context of a simple low-dimensional model. Such a model offers the obvious advantage of being computationally inexpensive, thus allowing for a much more detailed exploration of the model parameter space. It is also easier to tease out the chain of causality in a simple model, where there are far fewer variables to consider. Insights gained through such studies may then be used to inform future investigations using larger, more comprehensive models.

In section 2 we introduce the one-dimensional QBO model that will be the main focus of this study. Section 3 discusses the results of our experiments. A thorough examination of the parameter space of the model is conducted with regards to the effect of wave forcing and both the constant and annually varying components of tropical upwelling. We demonstrate that the addition of tropical upwelling creates broad regions of frequency locking where the QBO period remains an integer multiple of the annual cycle period. Outside of these locking regions, it is shown that the QBO period no longer remains constant in time, but instead exhibits a frequency modulation in which it cycles through a set of periods of varying structure and complexity. We further demonstrate that the addition of the annual cycle in tropical upwelling can actually help to generate a QBO in particular cases. In the context of increasing tropical upwelling, we investigate the evolution of the QBO period and suggest the possibility that the QBO period may adjust toward a 36-month period in a warming climate. Finally, in section 4, we discuss our results in the context of related work, and provide some observational evidence for cyclical behaviour of QBO periods in the real atmosphere.

2. Model description

We use the one-dimensional QBO model of Holton and Lindzen (1972) with the addition of tropical upwelling (Saravanan, 1990; Hampson and Haynes, 2004). Equatorial waves propagate vertically through the stratosphere and dissipate, depositing zonal momentum into the background flow. The resultant evolution of the zonal mean zonal wind, $\bar{u}(z,t)$, is given by

$$\frac{\partial \bar{u}}{\partial t} + w\frac{\partial \bar{u}}{\partial z} = -\frac{1}{\rho}\sum_i \frac{\partial \mathcal{F}_i}{\partial z} + \kappa\frac{\partial^2 \bar{u}}{\partial z^2}, \qquad (1)$$

where $\mathcal{F}_i$ is the wave momentum flux due to the ith wave, w is the strength of tropical upwelling, $\rho(z)$ is the mean density, and $\kappa = 0.3\,\mathrm{m^2\,s^{-1}}$ is vertical diffusion. Following Hampson and Haynes (2004), the vertical velocity is partitioned into the sum of constant and annually varying components:

$$w(z,t) = \left\{ w_c + w_a \cos\left(\frac{2\pi t}{360}\right)\right\} \exp\left\{\frac{z-z_t}{z_t - z_l}\right\},$$

where z_t and z_l are the top and bottom boundaries of the model respectively and for simplicity we have taken an annual cycle period of exactly 360 days. We will refer to w_c and w_a as the *constant* and *annually varying* components of tropical upwelling respectively. The atmosphere is assumed to be isothermal, with a density profile given by $\rho(z) = \rho_0 \exp(-z/H)$, where ρ_0 is the density at the bottom of the model and the density scale height is $H = 7.6\,\mathrm{km}$.

We assume the simplest possible wave forcing configuration of two identical gravity waves propagating through the stratosphere with equal and opposite phase speeds from z_l (Plumb, 1977). The wave momentum flux of each wave is given by Lindzen (1971) as

$$\frac{1}{\rho_0}\mathcal{F}_i(z,t) = F_i \exp\left\{-\int_{z_l}^{z} \frac{\mu N \alpha(z)}{k_i\{\bar{u}(z',t) - c_i\}^2}\,\mathrm{d}z'\right\}.$$

The individual wave momentum fluxes satisfy $F_1 = -F_2 = F$, and the corresponding wavespeeds and wavenumbers are given by $c_1 = -c_2 = 30\,\mathrm{m\,s^{-1}}$ and $k_1 = k_2 = 2\pi/40\,000\,\mathrm{km^{-1}}$ respectively. The thermal damping rate and buoyancy frequency are $\mu = 10^{-6}\,\mathrm{s^{-1}}$ and $N = 2.16\times10^{-2}\,\mathrm{s^{-1}}$, and $\alpha(z)$ is a non-dimensional dissipation profile given by

$$\alpha(z) = \begin{cases} 0.55 + 0.55\left(\frac{z-17}{6.5}\right), & z \le 30\,\mathrm{km}, \\ 1.65, & z > 30\,\mathrm{km}. \end{cases}$$

The equation of motion (1) is discretised over a non-uniform vertical grid of 200 points, and solved using an implicit Crank–Nicholson scheme with a time step of $\mathrm{d}t = 0.2$ days. Grid points are preferentially distributed toward the lower boundary of the model, where higher resolution is required to adequately resolve the sharp shear layers that sometimes form there. The boundary conditions are taken to be

$$\frac{\partial \bar{u}}{\partial z}(z_t) = \frac{\partial \bar{u}}{\partial z}(z_l) = 0.$$

This no-shear condition at the lower boundary is unusual and was chosen to reduce the model dependence on vertical diffusion for the break-up of shear zones at the bottom boundary.

This model makes several simplifying assumptions that do not hold in the real atmosphere. The use of only two discrete gravity waves to drive the model QBO is an obvious deficiency, given the broad spectrum of gravity, inertia-gravity, Kelvin and Rossby-gravity waves that are thought to drive the QBO in the real atmosphere (Baldwin *et al.*, 2001). The effect of the semi-annual oscillation, which is thought to have a role in synchronising the QBO winds in the upper stratosphere (Kuai *et al.*, 2009), has been neglected. Furthermore, the important effect of the meridional circulation on the QBO descent rate (Plumb and Bell, 1982) has been entirely ignored in this one-dimensional study.

The model described above is solved for various choices of F, w_c and w_a, over a vertical domain bounded by $z_l = 17\,\mathrm{km}$ and $z_t = 43\,\mathrm{km}$. Each simulation is run for at least $t = 180\,000$ days (500 years).

Figure 1 presents sample output from a test simulation with $F = 16.1\times10^{-3}\,\mathrm{m^2\,s^{-2}}$, $w_c = 0.3\,\mathrm{mm\,s^{-1}}$, and $w_a = 0.2\,\mathrm{mm\,s^{-1}}$. The model generates a reasonably realistic QBO with this choice of parameters. The oscillation has a period of exactly 24 months, with a peak amplitude of $26\,\mathrm{m\,s^{-1}}$ at around 30 km. However, both westerly and easterly wind regimes descend at the same rate, as a consequence of the use of identical wave sources to provide the forcing. The prominent asymmetry between easterly and westerly winds in the real stratosphere is also absent for the same reason. Further, the maximal wind amplitude does not decay below 30 km as is observed in the real stratosphere. Rather, the model maintains essentially the same maximal speed all the way down to the tropopause. This artifact is a consequence of the choice of a no-shear condition at the lower boundary.

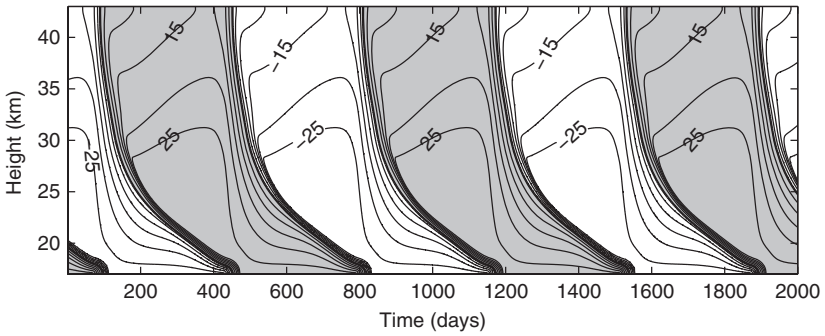

Figure 1. Zonal velocity contours from a sample run of the one-dimensional QBO model (1). Wave forcing is set at $F = 16.1\times10^{-3}\,\mathrm{m^2\,s^{-2}}$, and the constant and annually varying components of tropical upwelling are $w_c = 0.3\,\mathrm{mm\,s^{-1}}$ and $w_a = 0.2\,\mathrm{mm\,s^{-1}}$ respectively. Velocity contours are drawn in increments of $5\,\mathrm{m\,s^{-1}}$, and westerly wind regimes have been shaded.

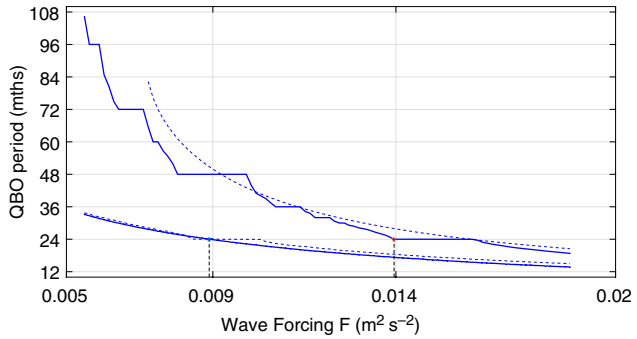

Figure 2. Average QBO period as wave forcing F is varied in two sets of 100 simulations with (top, solid line) and without (bottom, solid line) tropical upwelling. In the upwelling run we set $w_c = 0.3\,\mathrm{mm\,s^{-1}}$ and $w_a = 0.2\,\mathrm{mm\,s^{-1}}$; in the no-upwelling comparison we set both to 0. The dashed curves correspond to upwelling simulations where just one of w_a (top, dashed line) or w_c (bottom, dashed line) are set to 0 (with the other parameter retaining its non-zero value). The period of each simulation is computed by taking the Fourier spectrum of the zonal wind at $z = 24$ km and selecting the strongest spectral peak.

3. Experiments

3.1. *Influence of tropical upwelling on QBO period*

The response of the model QBO to increased wave forcing in the presence of tropical upwelling was considered. We ran a series of 100 simulations of the QBO, with tropical upwelling parameters set at $w_c = 0.3\,\mathrm{mm\,s^{-1}}$ and $w_a = 0.2\,\mathrm{mm\,s^{-1}}$. These numbers were chosen to represent approximately the strength of the present-day Brewer–Dobson circulation (Seviour *et al.*, 2012). Wave forcing was varied uniformly between $F = 5.5\times10^{-3}$ m^2 s^{-2} and $F = 18.8\times10^{-3}$ m^2 s^{-2}. The simulations were run in series from low to high values of F, such that the final condition of a simulation run at lower wave forcing was used as the initial condition for the next simulation at higher wave forcing. The period of the resulting QBO was then calculated by computing the Fourier spectrum of the zonal wind at $z = 24$ km, and selecting the frequency that gave the strongest spectral peak.

The variation of this QBO period with wave forcing is plotted in Figure 2 (solid line, top). This is compared with the QBO response in the absence of tropical upwelling (that is, with $w_c = w_a = 0$), which is also plotted (solid line, bottom).

In the case of no upwelling, the functional form of the curve reflects the inverse relationship between wave forcing strength and QBO period T as found by Plumb (1977):

$$T = \eta\frac{kc^3}{N\mu F},$$

where η is a dimensionless constant. When upwelling is included, the period of the QBO is significantly increased (for fixed values of F). The relative increase in period is greatest under conditions of weak forcing, and the gap in period reduces as wave forcing increases. We see that significant increases in wave forcing are required to maintain the QBO at a particular period under upwelling conditions. For example, a 24-month QBO requires that the wave forcing be around 50% larger in the presence of upwelling ($F = 13.9\times10^{-3}$ m^2 s^{-2}, as compared to $F = 8.9\times10^{-3}$ m^2 s^{-2} in the no-upwelling scenario; these points have been marked in Figure 2).

Furthermore, we see that the period of the QBO, though still monotonic, is no longer strictly decreasing as wave forcing increases. Instead, there are several plateau regions where the QBO period remains unchanged over a range of wave forcing, forming a structure reminiscent of the devil's staircase well-known from dynamical systems theory (Jensen *et al.*, 1984; Ott, 2002). Each plateau region represents a set of simulated QBOs that have an average period that is a rational multiple of the annual forcing period. The broadest plateaus represent integer multiples of 12 months, with plateaus at 24, 36, 48, 60, 72 and 96 months. An 84-month locking region presumably exists as well, but is too small to be resolved here given the rapid decrease of the QBO period with F when F is small. There is also a significant locking region corresponding to a 30-month QBO.

Regions corresponding to even-integer locking ratios (96, 72, 48, 24 months) tend to be broader than regions with odd-integer locking ratios (60 and 36 months). This is presumably because QBO periods that are even multiples of 12 months have constituent westerly and easterly phases with lengths that are also integer multiples of 12 months. Such an arrangement is more stable than that of the odd-multiple QBO periods, whose constituent westerly and easterly phases have lengths that are not integer multiples of 12 months.

The dashed curves in Figure 2 represent two sets of simulations in which either the constant or the annually varying component of the annual cycle was set to 0, with the other component set to retain its usual value ($w_a = 0.2\,\mathrm{mm\,s^{-1}}$ and $w_c = 0.3\,\mathrm{mm\,s^{-1}}$). In the case where $w_c = 0$ (bottom dashed curve), the period of the QBO returns to values that are comparable to the case where there is no upwelling at all. Due to the non-zero w_a, there is a wide locking region corresponding to a 24-month QBO. There is also a slight increase in the period of the QBO everywhere else. In the other case when $w_a = 0$ (top dashed curve), the period of the QBO becomes much longer due to the effect of the non-zero w_c. However, there are no plateaus corresponding to locking regions. Further, there is a minimum value of F below which the strength of the wave forcing is insufficient to overcome the effect of upwelling, resulting in the QBO being unable to form at all. For this reason, the curve has been truncated at small values of F.

3.2. *Quasi-periodic modulation of QBO periods*

We re-evaluate the results in section 3.1 using a different measure of the QBO period. Instead of calculating the Fourier spectrum,

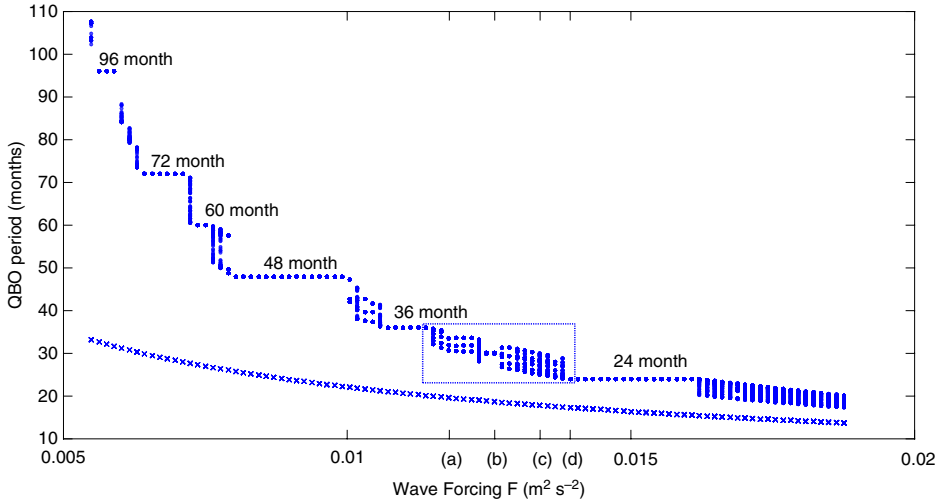

Figure 3. Individual QBO cycle lengths plotted against wave forcing, in the presence and absence of tropical upwelling. Each cycle length is defined by the time between the onset of westerly wind regimes at $z = 24$ km. Data points from the simulations with upwelling are plotted as dots, while those from simulations without upwelling are plotted as crosses. The region within the box is explored in greater detail in Figure 4.

we now simply measure the time between onsets of westerly wind regimes at $z = 24$ km. This gives a set of QBO cycle lengths for each model run that captures temporal changes in the QBO period over the length of the run. The Fourier-based QBO periods presented in Figure 2 are recovered as the average of this set of periods.

Figure 3 shows individual QBO cycle lengths over a range of wave forcing, with (dots) and without (crosses) upwelling. Each data point represents the period of an individual QBO cycle. From the plots we see that there is in fact much more variation in the length of individual periods than previously supposed. In the set of runs where there is no tropical upwelling, there is no temporal variation in QBO period; once transients have died away, the QBO adopts exactly one period throughout the simulation run at a given wave forcing. In contrast, when tropical upwelling is included in simulations, the only regions of wave forcing space where the QBO takes a single period are the aforementioned locking regions at integer multiples of the annual cycle. Outside of these areas, the QBO cycle length changes dynamically in time, and exhibits a complex pattern of variations that follows the general trend of the average QBO period shown in Figure 2 but with much more cycle-to-cycle variability.

In the light of these findings, we performed a second calculation to investigate the behaviour of QBOs with wave forcings in the region between the 36- and 24-month locking regions (denoted by the box in Figure 3). The number of simulations within this region was increased by a factor of 15, with a view to tease out the sensitivity of the QBO period to small changes to the wave forcing. The resulting QBO periods of each simulation were plotted against the corresponding wave forcing, and are presented in Figure 4. We see that the QBO period undergoes a complicated series of bifurcations as wave forcing increases. In particular, relatively small increases in wave forcing generate very large changes in the behaviour of the QBO period.

To illustrate some of the details of the observed behaviour, we consider four representative simulation runs, corresponding to wave forcing values of $F = 11.8\times10^{-3}$, 12.6×10^{-3}, 13.4×10^{-3} and 13.9×10^{-3} m^2 s^{-2}. (These have been marked (a)–(d) on the horizontal axis of Figure 3). For each simulation, we calculate the period of the individual QBO cycles and plot them sequentially across time in Figure 5. Histograms of the frequency of different QBO cycle lengths are then computed (Figure 6), as well as the frequency of westerly QBO regime onsets at 24 km for different phases of the annual cycle (Figure 7). Finally, we use delay embedding plots of the zonal wind time series at $z = 24$ km to reconstruct the geometry of phase space (Takens, 1981). These are presented in Figure 8, using a lag time of 300 days.

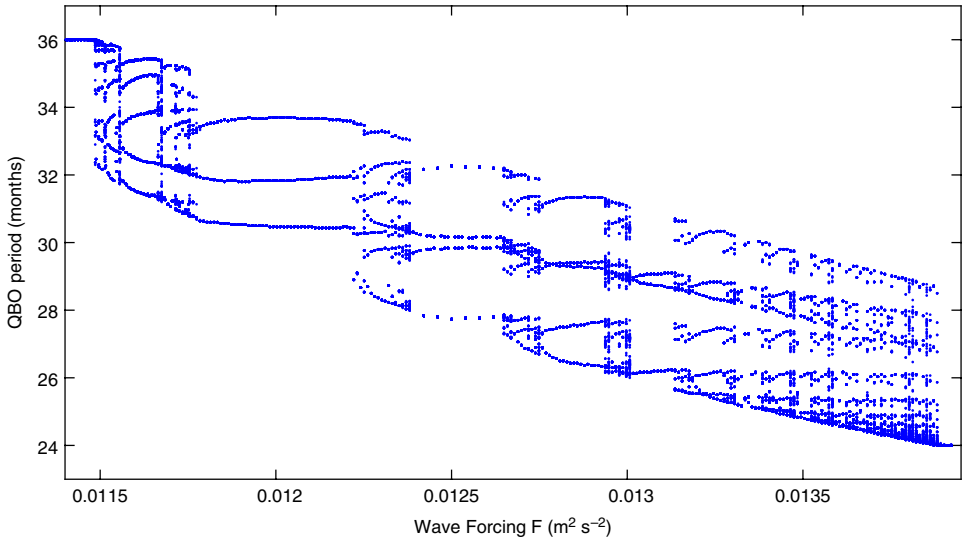

Figure 4. Recalculation of the QBO cycle periods for the region contained within the box in Figure 3. The resolution along the wave forcing axis has been increased by 15 times over the resolution in Figure 3. See text for details.

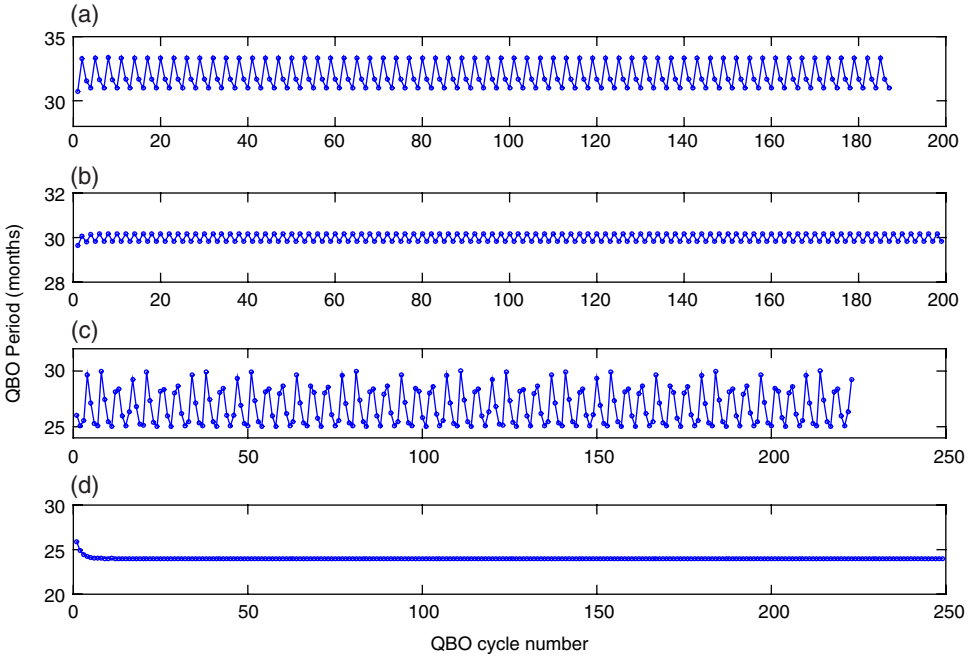

Figure 5. Evolution of QBO cycle length in the presence of tropical upwelling for four selected values of the wave forcing. Cycle length is measured by the time between onset of westerly QBO regimes at $z = 24$ km. The plots (a)–(d) correspond to wave forcing values of $F = 11.8\times10^{-3}$, 12.6×10^{-3}, 13.4×10^{-3} and 13.9×10^{-3} m^{2}s^{-2} respectively. The simulation time of each run is 500 years.

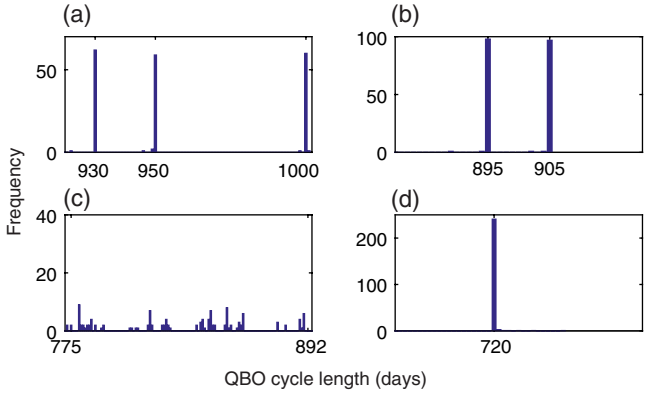

Figure 6. Histograms of the frequency of occurrence of different QBO cycle lengths, for each of the four cases considered in Figure 5.

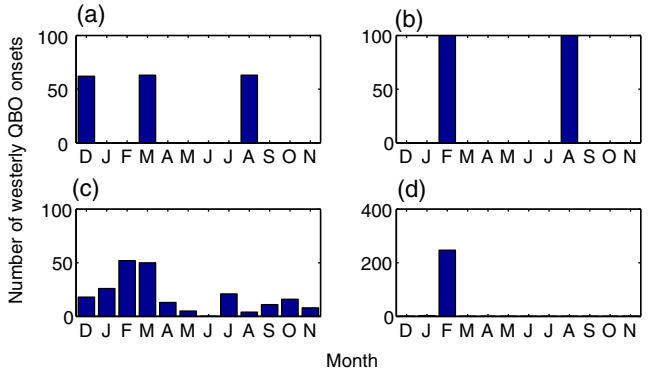

Figure 7. Number of QBO westerly onsets during different phases of the annual cycle, for each of the four cases from Figure 5.

It is clear from Figure 5 that variations in the QBO period are a robust feature of the simulations, and that they do not decay even over a half-millennial time-scale. Of the four simulations considered, only one obtains a regular period (Figures 5(d) and 6(d)). In this case ($F = 13.9\times10^{-3}$ m^2 s^{-2}), the intrinsic QBO period is suitably close to an integer multiple of 12 months, allowing the period of the QBO to adjust to an exact 2:1 synchronisation ratio with the annual cycle. As a result, the onset of westerlies at 24 km always occurs in the same month (Figure 7(d)). In general, we note that the onset month of QBO westerlies at a given height shifts to earlier months as wave forcing increases within a locking region (not shown).

In contrast, Figure 5(a) shows a QBO with a period that does not settle on a single value, but rather adopts a period-3 cycle in which it consistently alternates between periods of 930, 1000, and 950 days (Figure 6(a)). The sum of these periods is 2880 days, or exactly 8 years. This highlights a different type of synchronisation of the QBO with the annual cycle. The QBO period itself undergoes a frequency modulation, whereby several QBO cycles of different lengths combine in such a way that the sum of the periods is always a multiple of the annual cycle period. The number of cycles in the set can be deduced by counting the number of lines that would intersect a surface perpendicular to the reconstructed phase portrait of the oscillation (i.e. a Poincaré section). In this case there are three intersections (Figure 8(a)), reflecting the three discrete QBO periods.

Figure 5(b) shows a simulated QBO with very similar behaviour to the one discussed in the preceding paragraph. The major difference is that this QBO adopts a period-2 cycle instead of a period-3 cycle (Figure 8(b)). The period lengths are very similar at 895 and 905 days respectively, effectively specifying a QBO with a near-constant period of 30 months. The sum of the two distinct periods adds to 1800 days, or exactly 5 years.

The final example (Figure 5(c)) shows a QBO realisation that never quite settles down into a regular pattern of oscillation periods. The individual QBO cycles of this run take on a broad range of values between 26 and 30 months (Figure 6(c)). Also, the delay embedding plot (Figure 8(c)) is now much more filled-in than the other examples. This suggests that the simulated QBO possesses a broad-banded spectrum of periods. Westerly onsets occur throughout the year (Figure 7(c)), although there is a marked preference for onsets around February and March, with lower preference for westerly onset around May or June.

3.3. *QBO response to changes in w_c and w_a*

We considered the effect on QBO period of changes to both the wave forcing F and the constant component of tropical upwelling,

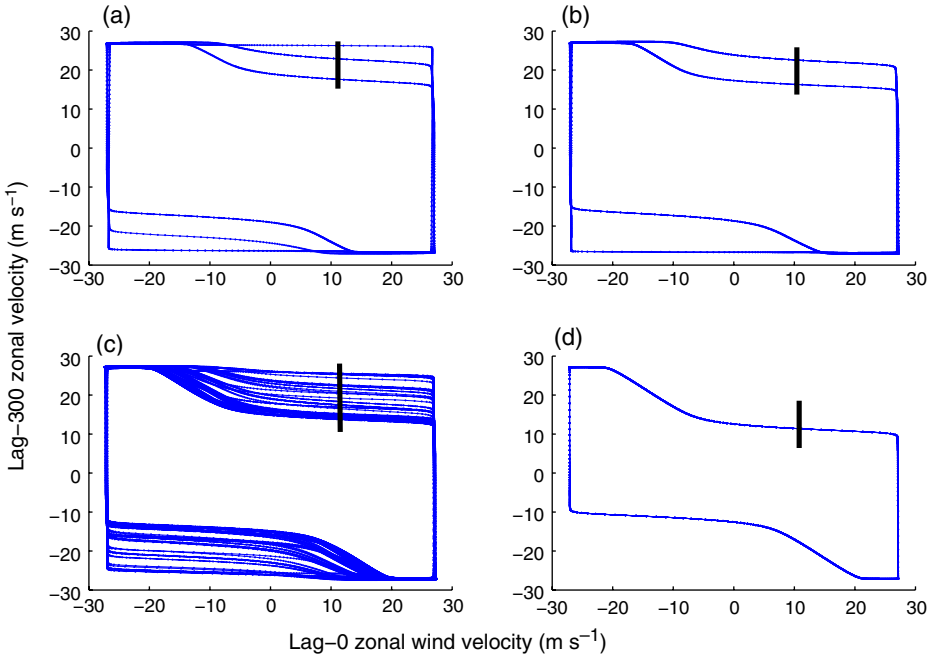

Figure 8. Delay embedding plots for each of the four cases from Figure 5, using zonal wind time series at $z = 24$ km. Poincaré sections of each plot are represented by short, dark, vertical lines. The number of different QBO periods in each case can be inferred by counting the number of distinct lines intersecting the corresponding Poincaré section.

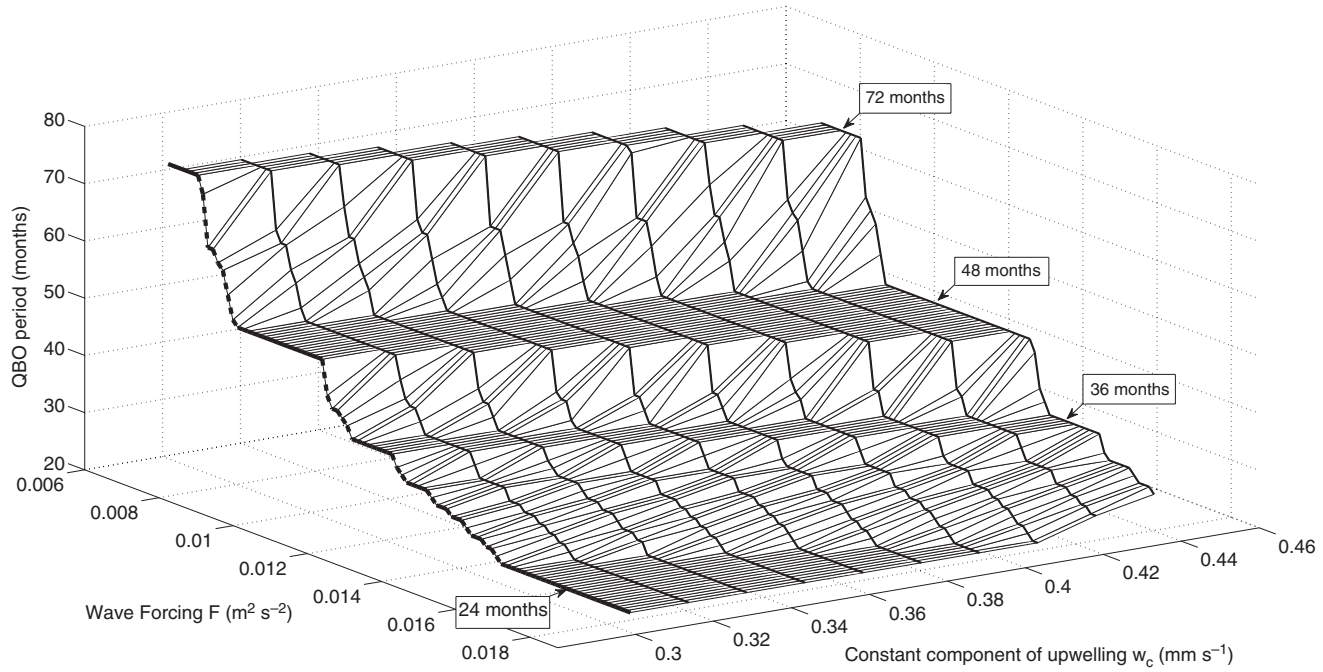

Figure 9. Surface plot of the variation of average QBO period with wave forcing (left axis) and the strength of the constant component of tropical upwelling (right axis). Plateaus in the surface – corresponding to integer year QBO periods – have been labelled. The bold dashed line is equivalent to the upper curve of Figure 2.

w_c. Ten different values of w_c were considered, starting with the present-day value of $w_c = 0.3\,\mathrm{mm\,s^{-1}}$ and increasing in 5% increments to $w_c = 0.43\,\mathrm{mm\,s^{-1}}$. As in section 3.1, the wave forcing F took 100 uniformly spaced values between 5.5×10^{-3} and 18.8×10^{-3} m^2 s^{-2}. The amplitude of the annual component in upwelling was held constant at $w_a = 0.2\,\mathrm{mm\,s^{-1}}$. Hence, a total of 1000 simulations were run.

Results of the runs described above are summarised in Figure 9, where the QBO period is plotted as a surface whose height depends on the values of F and w_c. The cross-section of this surface along $w_c = 0.3$ mm s^{-1} can be identified as the upper solid curve in Figure 2; it is marked with a dashed line in Figure 9.

In general we find that the QBO period increases as w_c increases, in line with our understanding of how increased upwelling impedes the descent of QBO shear zones (Dunkerton, 1991). A striking feature of Figure 9 is the presence of several shelves or plateaus on the period surface which clearly correspond to the locking regions discussed in section 3.1. Significant regions of annual synchronization occur at periods of 24, 36, 48 and 72 months. Within each locking region, increasing the strength of w_c at fixed values of F has the effect of delaying the onset of QBO westerlies to later months (not shown). As w_c is increased, we see that the width of the locking regions remain unchanged, but also that they shift horizontally and sit over higher values of wave forcing.

We also ran a separate set of experiments, very similar to the ones just described, but with w_c kept fixed at the present-day value of $w_c = 0.3$ mm s^{-1}, while the strength of the annual component of upwelling w_a was varied uniformly between 0 and 0.36 mm s^{-1}. Wave forcing variations are as described previously.

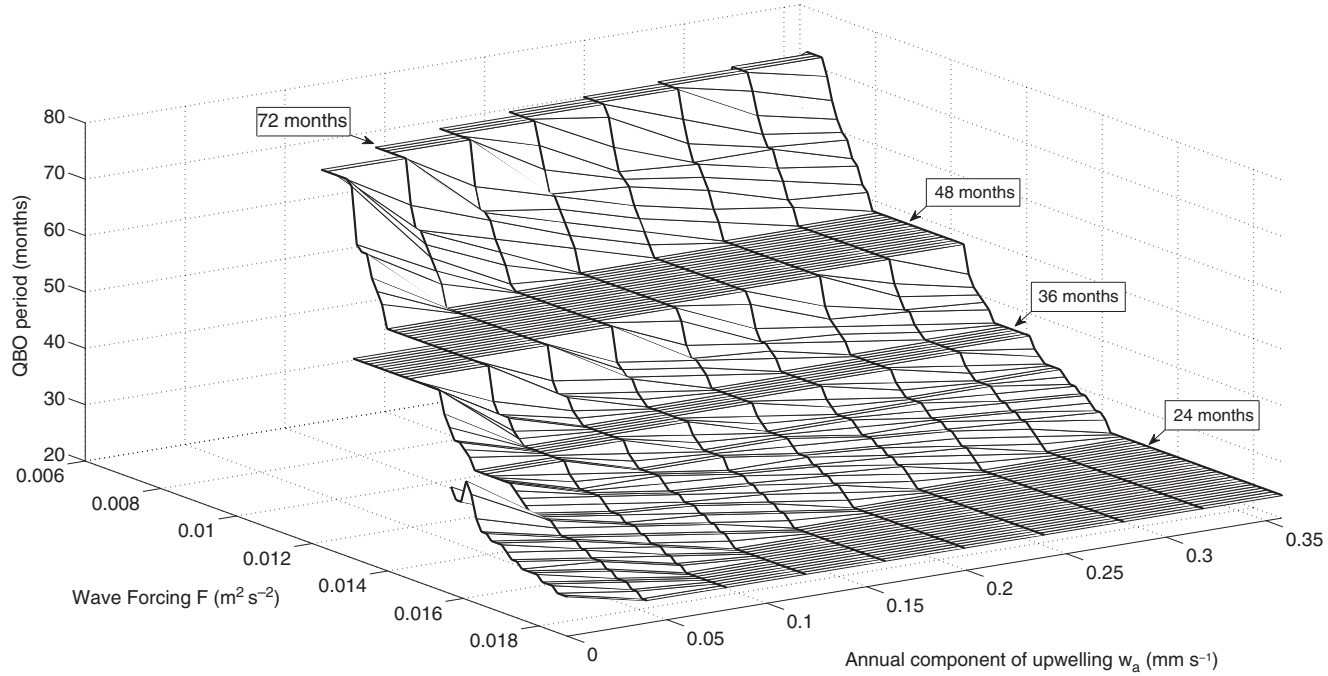

Figure 10. As Figure 9, but showing the strength of the annually varying component of tropical upwelling on the right axis.

Results of the simulations are displayed in Figure 10. We note that the model does not produce a QBO for small values of w_a and F. This is because the wave forcing is insufficient to overcome the effect of the mean upwelling. We have removed the results of simulations that do not produce a QBO.

From Figure 10 we confirm the presence of the same locking regions discussed earlier. In sensitivity tests (not shown), we find that increases in w_a at fixed F had a minimal impact on the onset month of the westerly QBO. However, as w_a is increased, we find that the QBO period tends to decrease. (This can be best seen by noticing that the lines linking the different locking regions in Figure 10 slant downwards). This suggests that w_a reduces the impact that w_c has on the descent rate of QBO shear zones, and that sufficiently strong values of w_a may be able to assist in QBO formation by mitigating the effect of w_c.

To investigate this possibility, we ran a series of 441 experiments, each with different values for F and w_a. In each simulation, the value of w_c was incrementally increased until just before the strength of the upwelling became large enough to prevent the formation of a QBO. A contour plot of this 'maximal-w_c' is presented in Figure 11. We see that there is a clear trade-off between F and w_a at a fixed maximal w_c. In other words, if the wave forcing is too weak to overcome the effect of a fixed mean upwelling, it may still be possible to generate a QBO by increasing the value of w_a to compensate, without having to increase the amount of parametrized wave forcing in the model.

3.4. *QBO response to increased tropical upwelling with constant wave forcing*

To study the effect of increased upwelling on the QBO at constant wave forcing, we considered four representative wave forcings ($F = (14.6, 15.3, 16.9, 18.2) \times 10^{-3}$ m^2 s^{-2}) and fixed $w_a = 0.2$ mm s^{-1} while letting w_c vary uniformly between 0.2 and 0.7 mm s^{-1}. We ran the simulations sequentially in w_c and computed the QBO periods using the Fourier method described in section 3.1.

Results of the average QBO period at each value of w_c are plotted in Figure 12 for each run. In all four cases, the QBO period tends to increase with increased upwelling over long periods. However, because of the tendency of the QBO to stay in a synchronised state with the annual cycle, the upwelling has to become quite strong before the period of a QBO in a frequency-locked regime begins to drift. For example, in the case when $F = 15.3 \times 10^{-3}$ m^2 s^{-2} (square markers), upwelling has to increase to at least 0.4 mm s^{-1} – a 25% increase on present-day values –before the QBO period begins to respond.

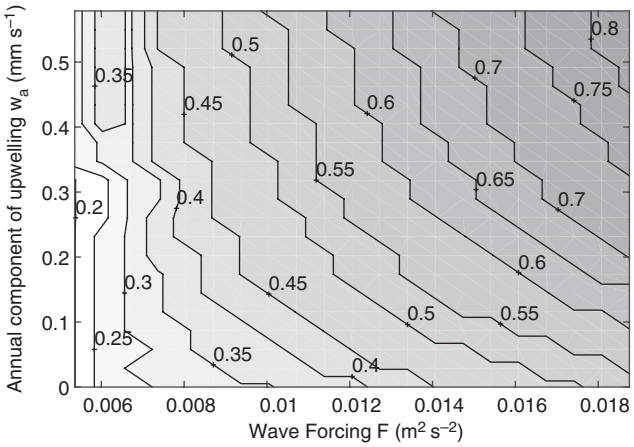

Figure 11. Contour map depicting the largest possible value of w_c (mm s^{-1}) at which a QBO can still form (for given values of F and w_a). Darker shades represent higher values of w_c.

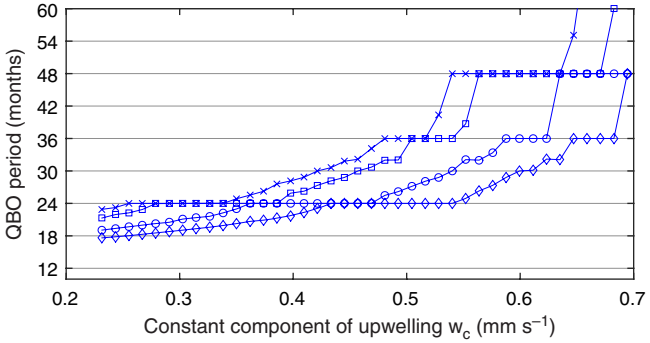

Figure 12. Increase in the average QBO period with increasing w_c. The amplitude of the annual cycle component of upwelling is kept constant at $w_a = 0.2$ mm s^{-1}. The four plots correspond to wave forcings F of 14.6×10^{-3} (crosses), 15.3×10^{-3} (squares), 16.9×10^{-3} (circles), and 18.2×10^{-3} (diamonds).

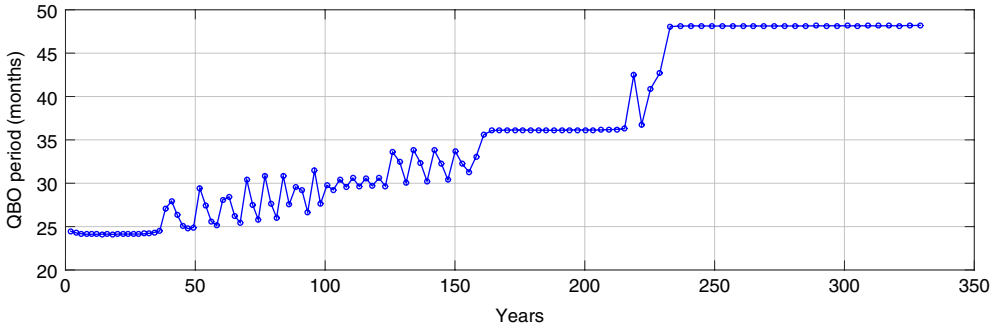

Figure 13. The changing length of individual QBO cycles over a span of ≈330 years as a result of continuously increasing upwelling. Wave forcing is fixed at $F = 14.6 \times 10^{-3}$ m^2 s^{-2}, and $w_a = 0.2$ mm s^{-1}. The constant component of upwelling w_c is allowed to change dynamically during the model run, increasing over present-day values at a rate of 3% per decade.

Furthermore, once the QBO period starts to drift, it eventually enters the 36-month locking region, where it again synchronises with the annual cycle. If w_c carries on increasing, a further period drift followed by entrainment to the 48-month locking region is also observed in some cases.

In our analysis thus far, we have not taken into account the findings presented in section 3.2 on the quasi-periodic behaviour of the QBO cycles, preferring to use the average QBO period metric instead. In the model reality, however, as upwelling is increased we expect the QBO period to adopt a more complicated set of frequency-modulated oscillation cycles than the smooth period changes of Figure 12 would suggest. To investigate this dynamical evolution of the QBO period, we took the simulation where $F = 14.6 \times 10^{-3}$ m^2 s^{-2} and ran it again. This time, as the model evolved, we set the value of w_c to increase dynamically at a rate of 3% per decade, in line with the predictions of GCM studies (Butchart, 2014). Once the model run was completed, the evolution of the QBO period was calculated using the time between westerly onsets at 24 km.

The resulting period evolution is plotted in Figure 13. As anticipated, the QBO period fluctuated quite considerably. For the first 36 years it remained in the 24-month locking region, fully synchronised with the annual cycle and unaffected by the increase in upwelling. When it finally drifted out of synchronicity, it almost immediately entered into a three-cycle pattern similar to the one discussed in section 3.2. After 62 years of period-3 cycles of a combined length of either 72 or 84 months, the QBO then transitioned to a two-cycle pattern for 25 years, in which its period was effectively 30 months. It then returned to a three-cycle for 35 years, this time with a combined cycle length of close to 96 months. At this point the period had drifted close enough to the 36-month locking region, and once again the QBO became synchronised to the annual cycle for 57 years. After clearing the 36-month locking region, it spent a short 13 years in transition before once again becoming entrained to the annual cycle. For the final 100 years until the end of the simulation, the QBO remained trapped in a 48-month oscillation.

4. Discussion

In this article we have demonstrated the possibility of exact synchronization of the QBO by the annual cycle, albeit in a highly idealised model. Exact synchronisation between the QBO and the annual cycle has not generally been reported in the real stratosphere (Dunkerton, 1990), although a recent article has presented observational evidence arguing in favour of this (Gabis, 2015).

The identification of discrete jumps in the QBO period at fixed values of the wave forcing has not been discussed by previous authors in the context of a one-dimensional QBO model. Our model results show that the QBO can adopt different periods from cycle to cycle that are not multiples of the annual cycle period, and yet are still influenced by the annual cycle in the sense that the set of unique periods at a given wave forcing sums to a multiple of 12 months. At present we do not have a theoretical explanation for the model behaviour, which seems to be an example of frequency locking under the influence of a periodic external force (e.g. Pikovsky *et al.*, 2003). A fuller appreciation of the behaviour of this model, understood in the context of dynamical systems theory, would be a useful study that is beyond the scope of the present article.

Table 1. Duration of westerly phases of the QBO at 50 hPa from 1951 to 2001, taken from Figure 1 of Hamilton (2002). The phases are listed in order of appearance (left to right, top to bottom), and have been separated into seven sets.

The right-hand column shows the sum of phase durations in each row.

Westerly phase duration (months)	Row sum
15, 14, 15, 10, 18,	72
21, 23, 13, 14,	71
14, 18, 17,	49
17, 19,	36
24,	24
20, 14,	34
17, 16, 13, 26,	72

As a simple test of whether the multiply periodic behaviour found in our model is seen in the real atmosphere, we consider the duration of westerly phases of the QBO in 50 hPa wind from 1953 to 2001 (Table 1). (These data were taken from Figure 1 of Hamilton, 2002) We consider westerly regimes in isolation, as they are not affected by the stalling that sometimes impedes the regular descent of easterly regimes (Baldwin *et al.*, 2001). In Table 1 the individual westerly periods have been listed in order of occurrence, but have been separated into seven sets. The sum of the periods of each set is also given in the table. Under this partitioning of the data, we see that the sum of periods in each set is either exactly or very close to a multiple of 12 months.

It has been suggested that the long-term cycle in the observed periods of the QBO are due to a 'multi-decadal oscillation' caused by an interaction between the QBO and the solar cycle (Salby and Callaghan, 2000). The results of our (admittedly idealised) modelling study suggest a possible alternative explanation to this phenomenon, which is that the multi-decadal oscillation of the QBO period is the result of the periodic adjustment of the QBO phase due to its interaction with the annual cycle in tropical upwelling. However, much more work would be required before one could make a definitive statement either way as to the cause of the multi-decadal oscillation.

We have shown that the frequency locking between the QBO and the annual cycle in tropical upwelling allows for the creation of 24-, 30-, and 36-month QBO periods. These are the same QBO periods identified by Read and Castrejón-Pita (2012) in their study of the QBO period in the ERA-40 and ERA-Interim reanalysis datasets produced by the European Centre for Medium-range Weather Forecasts. Our findings reinforce the notion that the observed synchronization between the QBO and the stratopause

semi-annual oscillation (SAO; Dunkerton and Delisi, 1997; Kuai *et al.*, 2009; Read and Castrejón-Pita, 2012; Krismer *et al.*, 2013) does not necessarily imply a causal dynamical link between the two oscillations, but may in fact simply be due to the independent synchronization of both wind systems to the underlying annual cycle.

In the real atmosphere the QBO is thought to be generated by a wave spectrum made up of Kelvin waves, mixed Rossby-gravity waves, and gravity waves. The exact make-up of this wave spectrum, and the relative importance of the large-scale and small-scale components, is still poorly understood (Baldwin *et al.*, 2001). We have not considered any of these issues, and have chosen to focus on a highly idealised wave spectrum that is constant in time and only has two wave components. This constrains the direct applicability of our results to the real atmosphere. Nevertheless, even in this simple setting, our findings highlight that the pattern of QBO periods under the influence of the annual cycle is very rich (Figure 3). Further, relatively small variations in the wave forcing lead to quite drastic variations in the dynamics of the QBO period (Figure 4). This implies that our ability to predict the long-term QBO period (Scaife *et al.*, 2014) may be quite limited due to the sensitivity of the QBO period to variations in the strength of upwelling and wave forcing as a result of both natural variability and anthropogenic climate forcing.

Gravity wave sources in the real atmosphere are also time-varying, and display seasonal and interannual variations (Fritts and Alexander, 2003). Geller *et al.* (1997) have demonstrated that the QBO displays complex behaviour when wave forcing is time-varying in a one-dimensional model. In particular, they showed that the introduction of a sinusoidal variation on the wave forcing results in phase locking of the QBO to the period of the variation in the forcing. Although our model does not take such variations into account, it seems plausible that the imposition of an annual cycle in the wave forcing would the strengthen the synchronization of the QBO to the annual cycle.

In the context of a warming climate, Kawatani and Hamilton (2013) presented evidence of a weakening trend in the amplitude of the QBO winds in the lower stratosphere, and used this to infer a strengthening of the Brewer–Dobson circulation. In our study of the QBO response to increased tropical upwelling, we do not consider changes to the QBO amplitude as our prescription of the wave forcing is too simplistic. Instead, we focus on the resulting changes to the QBO period. Our results suggest that the period of the QBO will increase in line with the strengthening of the mean amplitude of the Brewer–Dobson circulation that is predicted by most GCMs (Butchart, 2014). The current QBO-resolving GCMs, however, are not consistent in their predictions of the future trend of the QBO period in a warming climate. Indeed, two models (MPI-ESM-MR and HadGEM2-CC) actually predict a *decrease* in the period of the QBO (Figure S8 in the Supplementary Information of Kawatani and Hamilton, 2013). This decrease could be due to an increase in the annual component of tropical upwelling, which has been shown to reduce the period of the QBO in our model (Figure 10). This would be consistent with the predicted increase in mean tropical upwelling if the future increasing trend in upwelling varies with season, so that the Northern Hemisphere winter trend is stronger than the Southern Hemisphere winter trend.

Our results also suggest that it might be possible to use the strength of the amplitude of the annual cycle in tropical upwelling to help to generate a QBO in GCMs. Many GCMs currently struggle to generate an internal QBO, partly due to the difficulties in generating sufficient wave forcing in order to overcome the effect of mean tropical upwelling. Based on our results, a possible strategy to mitigate this problem would be to enhance the hemispheric contrast in extratropical wave generation in the models. This would strengthen the annual cycle in tropical upwelling, which would reduce the amount of wave activity necessary to generate a QBO in the model (Figure 11).

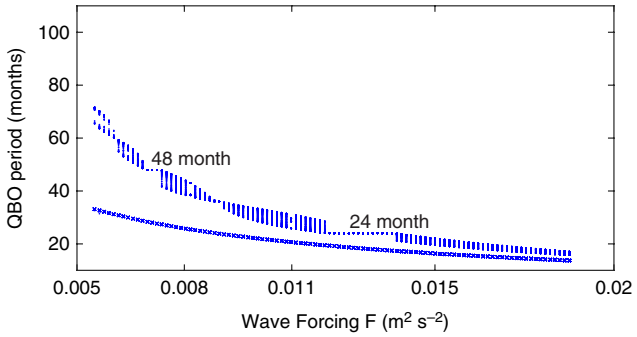

Figure 14. As Figure 3, but using a no-slip condition at the lower boundary instead of the no-shear condition. See text for details.

The QBO period in our model undergoes a series of oscillations as the strength of tropical upwelling increases, and it eventually enters the 36-month locking region (Figure 13). A firm prediction as to whether or not increased upwelling will eventually lead to exact frequency locking of the QBO at 36 months sometime in the next century cannot be made with any precision from this simplified model. However, our findings do underscore the crucial role that the annual cycle in the Brewer–Dobson circulation plays in determining the evolution of the QBO period in future decades. The importance of realising a robust representation of this feature in GCMs should be emphasised.

A similar model of the QBO was used by Hampson and Haynes (2004) (hereafter referred to as HH), who investigated phase alignment of the QBO due to the annual cycle in both a 1D model and a 3D mechanistic model. The 1D model in their study also produced a locking region in the wave forcing space, around 24 months. However, they did not find a locking region at 36 months, in contrast to our results. The only substantial difference between their model and ours is the use of different lower boundary conditions: we have chosen to use a no-shear condition at the lower boundary, while HH use a no-slip condition. To test whether this difference in the lower boundary condition could account for the difference in our results, we recomputed our simulations using a no-slip condition at the lower boundary. Results are displayed in Figure 14. We find close agreement with the results of HH when the no-slip condition is imposed (comparing Figure 14 to Figure 10 of HH). The 24-month locking region persists, and there is also a locking region at 48 months, outside of the range of values presented by HH. Away from these two locking regions, the QBO tends to adopt a continuous set of periods. Notably, the 36-month locking region has disappeared; there is now only a single value of wave forcing (at present resolution) for which the QBO period is exactly 36 months. The spread of QBO periods increases with increasing distance from this point. There are also a few cases where the QBO adopts a discrete set of periods. For example, there is a period-2 cycle at $F = 8.1\times10^{-3}$ m^2 s^{-2} and a period-3 cycle at $F = 11.0\times10^{-3}$ m^2 s^{-2}. However, these are much less prevalent.

The imposition of a no-slip condition at the lower boundary enforces too strong a kinematic constraint on the flow, effectively forcing the QBO winds to zero at the tropopause. The result of this constraint tends to be the creation of very sharp shear zones at the bottom of the model. These narrow shear bands introduce spurious numerical oscillations into the model results, and these are difficult to prevent even at extremely high vertical resolution. It is likely that the seemingly continuous QBO periods and the disappearance of the 36-month locking region observed in the no-slip case can be attributed to this numerical noise, keeping in mind that locking regions that are odd multiples of the forcing period are less stable than locking regions that are even multiples.

The no-shear condition, in contrast, does not place such an exacting constraint on the flow at the lower boundary. As a result, sharp shear zones do not form in this model configuration, which results in a smoother QBO evolution. This allows for the

subtle details of the QBO period dynamics to be observed much more clearly. The downside of this approach, however, is that the model no longer has stratospheric winds decaying to zero near the bottom boundary. Of course, in the real stratosphere there is no boundary at the tropopause at all, and the fact that observed QBO winds weaken there is a dynamical effect that is related to weaker wave forcing in that region of the atmosphere. It would seem that the way to simulate the dynamics properly would be to use the no-shear condition coupled with a more realistic parametrization of the wave spectrum. Such an extension would be an interesting work for the future.

Acknowledgements

PLR and SMO are supported by the UK Natural Environment Research Council (NERC) and the UK National Centre for Atmospheric Science (NCAS) respectively. KR and SMO gratefully acknowledge generous travel support from NERC (QBOnet) and the Stratosphere-troposphere Processes and their Role in Climate (SPARC) Project of the World Climate Research Programme (WCRP). The authors would like to thank Lesley Gray, James Anstey and William Seviour for insightful discussions over the course of this work. Thanks also go to the two anonymous referees for providing useful feedback and suggestions to improve the article.

References

Baldwin M, Gray LJ, Dunkerton T, Hamilton K, Haynes P, Randel W, Holton J, Alexander M, Hirota I, Horinouchi T, Jones DBA, Kinnersley JS, Marquardt C, Sato K, Takahashi M. 2001. The quasi-biennial oscillation. *Rev. Geophys.* **39**: 179–229, doi: 10.1029/1999RG000073.

Butchart N. 2014. The Brewer–Dobson circulation. *Rev. Geophys.* **52**: 157–184.

Butchart N, Scaife A, Bourqui M, De Grandpré J, Hare S, Kettleborough J, Langematz U, Manzini E, Sassi F, Shibata K, Shindell D, Sigmond M. 2006. Simulations of anthropogenic change in the strength of the Brewer–Dobson circulation. *Clim. Dyn.* **27**: 727–741, doi: 10.1007/s00382-006-0162-4.

Dunkerton T. 1990. Annual variation of deseasonalized mean flow acceleration in the equatorial lower stratosphere *J. Meteorol. Soc. Jpn.* **68**: 499–508.

Dunkerton T. 1991. Nonlinear propagation of zonal winds in an atmosphere with Newtonian cooling and equatorial wavedriving. *J. Atmos. Sci.* **48**: 236–263.

Dunkerton T, Delisi D. 1985. Climatology of the equatorial lower stratosphere. *J. Atmos. Sci.* **42**: 376–396.

Dunkerton T, Delisi D. 1997. Interaction of the quasi-biennial oscillation and stratopause semiannual oscillation. *J. Geophys. Res.* **102**: 26107–26116, doi: 10.1029/96JD03678.

Fritts D, Alexander M. 2003. Gravity wave dynamics and effects in the middle atmosphere. *Rev. Geophys.* **41**: 1003, doi: 10.1029/2001RG000106.

Gabis I. 2015. The validity of long-term prediction of quasi-biennial oscillation (QBO) as a proof of the exact seasonal synchronization of the equatorial stratospheric QBO cycle. *J. Atmos. Sol. Terr. Phys.* **124**: 44–58.

Garcia RR, Randel WJ. 2008. Acceleration of the Brewer–Dobson circulation due to increases in greenhouse gases. *J. Atmos. Sci.* **65**: 2731–2739.

Geller M, Shen W, Zhang M, Tan W. 1997. Calculations of the stratospheric quasi-biennial oscillation for time-varying wave forcing. *J. Atmos. Sci.* **54**: 883–894.

Hamilton K. 2002. On the quasi-decadal modulation of the stratospheric QBO period. *J. Clim.* **15**: 2562–2565.

Hampson J, Haynes P. 2004. Phase alignment of the tropical stratospheric QBO in the annual cycle. *J. Atmos. Sci.* **61**: 2627–2637.

Holton J, Lindzen R. 1972. An updated theory for the quasi-biennial cycle of the tropical stratosphere. *J. Atmos. Sci.* **29**: 1076–1080.

Jensen MH, Bak P, Bohr T. 1984. Transition to chaos by interaction of resonances in dissipative systems. I. Circle maps. *Phys. Rev. A* **30**: 1960.

Kawatani Y, Hamilton K. 2013. Weakened stratospheric quasi-biennial oscillation driven by increased tropical mean upwelling. *Nature* **497**: 478–481.

Kinnersley J, Pawson S. 1996. The descent rates of the shear zones of the equatorial QBO. *J. Atmos. Sci* **53**: 1937–1949.

Krismer T, Giorgetta M, Esch M. 2013. Seasonal aspects of the quasi-biennial oscillation in the Max Planck Institute earth system model and ERA-40. *J. Adv. Model. Earth Syst.* **5**: 406–421.

Kuai L, Shia R, Jiang X, Tung K, Yung Y. 2009. Non-stationary synchronization of equatorial QBO with SAO in observations and a model. *J. Atmos. Sci.* **66**: 1654–1664.

Li X, Read PL, Andrews D. 1997. Mode selection, wave breaking and parametric sensitivity in the quasi-biennial oscillation. *Q. J. R. Meteorol. Soc.* **123**: 2041–2068.

Lindzen R. 1971. Equatorial planetary waves in shear: Part I. *J. Atmos. Sci.* **28**: 609–622.

Lindzen R, Holton J. 1968. A theory of the quasi-biennial oscillation. *J. Atmos. Sci.* **25**: 1095–1107.

Ott E. 2002. *Chaos in Dynamical Systems*. Cambridge University Press: Cambridge, UK.

Pascoe C, Gray LJ, Crooks S, Juckes M, Baldwin M. 2005. The quasi-biennial oscillation: Analysis using ERA-40 data. *J. Geophys. Res.* **110**: D08105, doi: 10.1029/2004JD004941.

Pikovsky A, Rosenblum M, Kurths J. 2003. *Synchronization: A Universal Concept in Nonlinear Sciences*, Vol. 12. Cambridge University Press: Cambridge, UK.

Plumb R. 1977. The interaction of two internal waves with the mean flow: Implications for the theory of the quasi-biennial oscillation. *J. Atmos. Sci.* **34**: 1847–1858.

Plumb R, Bell R. 1982. A model of the quasi-biennial oscillation on an equatorial beta-plane. *Q. J. R. Meteorol. Soc.* **108**: 335–352.

Read PL, Castrejón-Pita A. 2012. Phase synchronization between stratospheric and tropospheric quasi-biennial and semi-annual oscillations. *Q. J. R. Meteorol. Soc.* **138**: 1338–1349.

Salby M, Callaghan P. 2000. Connection between the solar cycle and the QBO cycle: The missing link. *J. Clim.* **13**: 2652–2662.

Saravanan R. 1990. A multiwave model of the quasi-biennial oscillation. *J. Atmos. Sci.* **47**: 2465–2474.

Scaife AA, Athanassiadou M, Andrews M, Arribas A, Baldwin M, Dunstone N, Knight J, MacLachlan C, Manzini E, Müller WA, Smith D, Stockdale T, Williams A. 2014. Predictability of the quasi-biennial oscillation and its northern winter teleconnection on seasonal to decadal timescales. *Geophys. Res. Lett.* **41**: 1752–1758, doi: 10.1002/2013GL059160.

Schirber S, Manzini E, Krismer T, Giorgetta M. 2015. The quasi-biennial oscillation in a warmer climate: Sensitivity to different gravity wave parameterizations. *Clim. Dyn.* **45**: 825–836, doi: 10.1007/s00382-014-2314-2.

Seviour WJ, Butchart N, Hardiman SC. 2012. The Brewer–Dobson circulation inferred from ERA-Interim. *Q. J. R. Meteorol. Soc.* **138**: 878–888.

Takens F. 1981. *Detecting Strange Attractors in Turbulence*. Springer: Berlin.

Yao W, Jablonowski C. 2015. Idealized quasi-biennial oscillations in an ensemble of dry GCM dynamical cores. *J. Atmos. Sci.* **72**: 2201–2226.

Yulaeva E, Holton JR, Wallace JM. 1994. On the cause of the annual cycle in tropical lower-stratospheric temperatures. *J. Atmos. Sci.* **51**: 169–174.